Dystroglycan Function Requires Xylosyl- and Glucuronyltransferase Activities of LARGE

Kei-ichiro Inamori,[1]* Takako Yoshida-Moriguchi,[1]* Yuji Hara,[1] Mary E. Anderson,[1] Liping Yu,[2] Kevin P. Campbell[1]†

Posttranslational modification of alpha-dystroglycan (α-DG) by the like-acetylglucosaminyltransferase (LARGE) is required for it to function as an extracellular matrix (ECM) receptor. Mutations in the *LARGE* gene have been identified in congenital muscular dystrophy patients with brain abnormalities. However, the precise function of LARGE remains unclear. Here we found that LARGE could act as a bifunctional glycosyltransferase, with both xylosyltransferase and glucuronyltransferase activities, which produced repeating units of [−3-xylose−α1,3-glucuronic acid-β1−]. This modification allowed α-DG to bind laminin-G domain−containing ECM ligands.

Protein glycosylation is important in determining cellular localization, modulating structural conformation, and providing recognition sites for other molecules (*1*). Dystroglycan (DG) is a highly glycosylated basement membrane receptor involved in a variety of physiological processes that maintain skeletal muscle membrane integrity, as well as central nervous system structure and function; it also serves as a receptor for Old World arenaviruses. Composed of a cell surface α subunit and a transmembrane β subunit (*2*), α-DG acts as a receptor for laminin-G domain–containing extracellular matrix (ECM) proteins such as laminin, agrin, and neurexin (*3*). α-DG undergoes *N*-glycosylation, mucin-type *O*-glycosylation, and *O*-mannosylation, and a yet-to-be identified modification of a phosphorylated *O*-mannosyl glycan is believed to be responsible for ligand binding (*4*). Perturbed glycosylation can lead to reduced ligand binding by α-DG and is a common pathologic feature among several congenital and limb-girdle muscular dystrophies. Mutations in the *LARGE* gene (*5*) and several others involved in *O*-mannosyl glycan synthesis have been identified in these disorders (*6*). The overexpression of LARGE enhances functional

modification of α-DG, as well as laminin binding in cultured cells (*7*). Moreover, it circumvents defects in the modification of α-DG in cells from patients with several genetically distinct types of congenital muscular dystrophies (*8*). Although LARGE has been implicated in the postphosphoryl modification pathway that assembles the laminin-binding moiety onto the phosphorylated *O*-mannose of α-DG, its molecular role and the laminin binding epitope remain to be identified.

We investigated the LARGE-dependent modification on α-DG by performing compositional sugar analysis of the recombinant α-DG produced in LARGE-expressing human embryonic kidney (HEK) 293 cells (fig. S1). Samples were treated with glycosidases to eliminate glycans unrelated to the laminin-binding moiety (*4*). We detected: (i) known compositional sugars of the α-DG *O*-mannosyl glycan—specifically *N*-acetylglucosamine (GlcNAc), galactose (Gal), *N*-acetylgalactosamine (GalNAc), and mannose (Man) (*4*); (ii) glucose (Glc), which was likely a contaminant; and (iii) substantial amounts of glucuronic acid (GlcA) and xylose (Xyl) (Fig. 1A). GlcA and Xyl are essential components of heparan sulfate (HS) and chondroitin-dermatan sulfate (CS-DS) glycosaminoglycans (GAGs), whose biosynthesis is initiated by linkage of tetrasaccharide GlcAβ1-3Galβ1-3Galβ1-4Xylβ1- to proteoglycan core proteins. Notably, GAGs are not required for α-DG to bind laminin (*9*, *10*) (fig. S2).

We tested whether xylosylation unrelated to GAG formation is involved in functional modification of α-DG by assessing uridine 5′-diphosphate (UDP)–xylose synthase 1 (UXS1)–deficient Chinese hamster ovary (CHO) cells (line pgsI-208), which are deficient in GAG synthesis because they

Fig. 1. Xylosylation is required for functional modification of α-DG. (**A**) Compositional sugar analysis by gas chromatography-MS with trimethylsilyl derivatization using α-DG produced by LARGE-overexpressing HEK293 cells digested with peptide: *N*-glycosidase F, *O*-glycosidase, and neuraminidase. Peaks shown in red represent Xyl, those in blue represent GlcA, and numbers indicate 1, Man; 2, Gal; 3, Glc; 4, GlcNAc; 5, GalNAc; and 6, inositol (internal control). Some of the detected Gal was derived from the Jacalin elution buffer we used for the purification. (**B**) Flow cytometry of WT or UXS1-deficient (pgsI-208) CHO cells surface stained with antibodies against the laminin-binding epitope of α-DG (IIH6), the α-DG core protein (CORE), or heparan sulfate (HS). Dashed line, secondary antibody alone. (**C**) Functional modification of α-DG in cells overexpressing UXS1. (Left) Immunoblotting or laminin overlay (OL) assays of glycoproteins. *M*r, relative molecular mass. Asterisk indicates nonfunctional α-DG that appeared as a sharp band because of hypomodification by CORE staining. (Right) Flow cytometry for surface staining with HS or IIH6. (**D**) Immunoblotting for IIH6 and β-DG–specific antibody reactivity in WT and pgsI-208 cells with or without overexpression of LARGE. (**E**) Immunoblotting for IIH6, CORE, or β-DG–specific antibody reactivity in LARGE-expressing WT cells treated with or without Xyl-α-pNP.
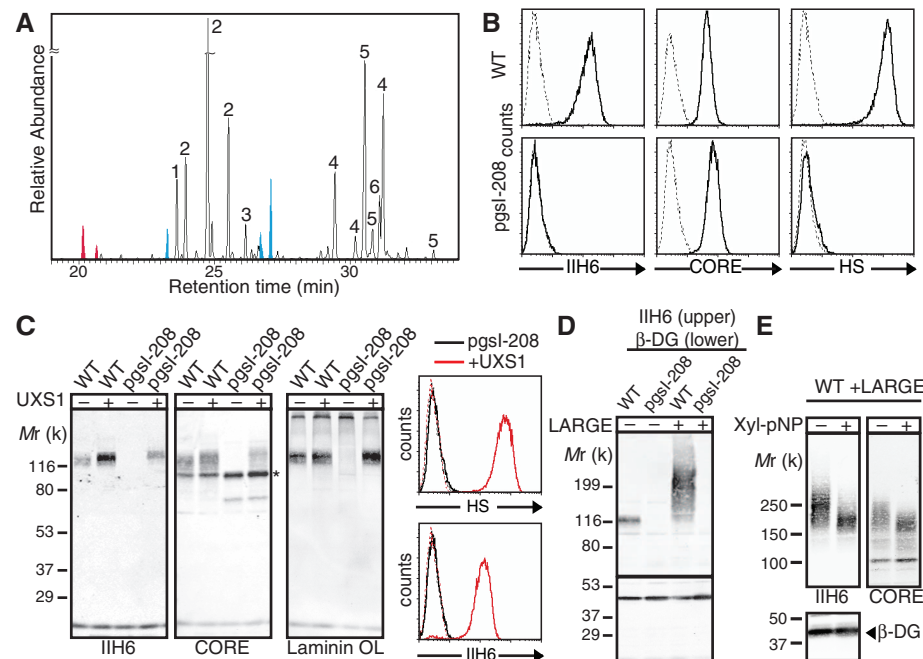
lack UDP-Xyl (11). Immunoblotting with IIH6 (an antibody that recognizes the laminin-binding form of α-DG), laminin overlay of wheat germ agglutinin–enriched proteins (glycoproteins), and flow cytometric analysis revealed that these cells were defective in synthesis of the functional modification of α-DG (Fig. 1, B and C). Ectopic expression of UXS1 in pgsI-208 cells rescued HS-GAG synthesis, as well as the IIH6 reactivity and laminin-binding ability of α-DG (Fig. 1C). In contrast, overexpression of LARGE in these cells did not overcome the defect (Fig. 1D). Thus, xylosylation may be required for formation of the acceptor substrate on which LARGE acts, and/or LARGE itself may be involved in the transfer of Xyl to α-DG. Xylosides with hydrophobic moieties that help penetrate lipid bilayers are widely used to inhibit certain glycosyltransferases acting on Xyl, because they serve as artificial acceptors (12). Given that one of the two domains of LARGE belongs to glycosyltransferase family 8 (GT8), whose members generate products with an α-linked glycosidic bond (13), we tested α-D-xyloside for the ability to inhibit functional modification of α-DG. Indeed, treat-

ment of LARGE-expressing CHO cells with p-nitrophenyl-α-D-xyloside (Xyl-α-pNP) reduced α-DG glycosylation (Fig. 1E). Thus xyloside may compete against endogenous α-DG bearing an α-linked Xyl for LARGE-dependent modification.

Next, we examined the enzymatic activity of LARGE with respect to Xyl-α-pNP as the acceptor, using a secreted form of LARGE that lacks its transmembrane domain (LARGEdTM). Purified LARGEdTM (fig. S3) was incubated with Xyl-α-pNP and each donor substrate, and the reaction products were separated by high-performance liquid chromatography (HPLC). A unique peak was detected only when UDP-GlcA was used as the donor (Fig. 2A for UDP-GlcA and fig. S4 for other donors). This activity was specific to α-linked Xyl (fig. S5). We purified the product (fig. S6) and analyzed it by mass spectrometry (MS). The MS/MS fragmentation pattern of a parent ion at mass/charge ratio, m/z, of 446.25 [M-H]⁻ demonstrated that GlcA was attached to Xyl-α-pNP (Fig. 2B and fig. S7). Because LARGE showed glucuronyltransferase (GlcA-T) activity toward α-linked Xyl and has two glycosyltransferase-like domains, we hy-

pothesized that it could also act on a nonreducing terminal GlcA. When 4-methylumbelliferyl-β-D-glucuronide (GlcA-β-MU) was used as an acceptor, a unique peak was observed only with UDP-Xyl (Fig. 2C for UDP-Xyl and fig. S8 for other donors); the attachment of Xyl to GlcA-β-MU was confirmed by MS (Fig. 2D and fig. S9).

Because mutations in the LARGE Asp-X-Asp (DXD; X, any amino acid) motifs (Fig. 2E), which are highly conserved across glycosyltransferases, lead to failed functional modification of α-DG (14), we generated constructs with such mutations for further testing of LARGE glycosyltransferase activity. In the case of the DXD1 mutant in which Asn replaces Asp at two sites (D242N/D244N), GlcA-T activity was comparable to that in wild type (WT), whereas Xyl-T activity was undetectable (Fig. 2F). In the DXD3 mutant D563N/D565N, in contrast, Xyl-T activity, but not GlcA-T activity, was present (Fig. 2F). Thus, LARGE is a bifunctional glycosyltransferase composed of two distinct catalytic domains, Xyl-T and GlcA-T.

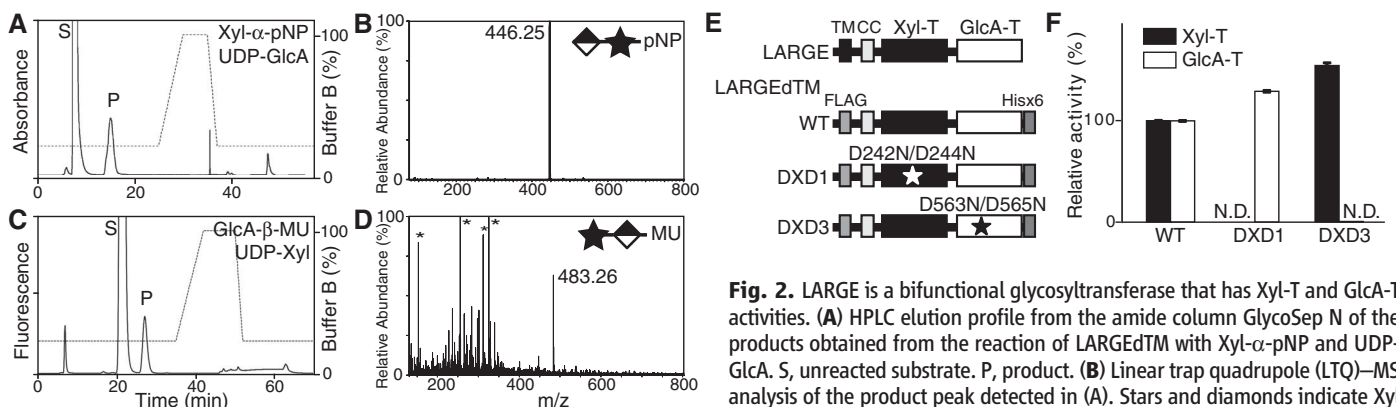Negatively charged oligosaccharides likely contribute to binding between α-DG and laminin

Fig. 2. LARGE is a bifunctional glycosyltransferase that has Xyl-T and GlcA-T activities. (**A**) HPLC elution profile from the amide column GlycoSep N of the products obtained from the reaction of LARGEdTM with Xyl-α-pNP and UDP-GlcA. S, unreacted substrate. P, product. (**B**) Linear trap quadrupole (LTQ)–MS analysis of the product peak detected in (A). Stars and diamonds indicate Xyl and GlcA, respectively. MS/MS fragmentation pattern (fig. S7) confirmed that the ion with m/z of 446.3 [M-H]⁻ is Xyl-α-pNP with an added GlcA. (**C**) HPLC elution profile from GlycoSep N of the products obtained from the reaction of LARGEdTM with GlcA-β-MU and UDP-Xyl. (**D**) As in the legend to (B), for the product isolated from the reaction analyzed in (C). The MS/MS fragmentation pattern (fig. S9) confirmed that the ion with m/z of 483.3 [M-H]⁻ is GlcA-β-MU with an added Xyl. Asterisks indicate background ions. (**E**) Schematic representation of the WT and DXD mutants of LARGEdTM constructs used in the assay. The locations of the mutations in the DXD motifs are symbolized by stars. (**F**) GlcA-T and Xyl-T activities of WT and mutant LARGEdTMs. Relative activity (%) with respect to WT, and the standard deviation in triplicate experiments, are shown. TM, transmembrane domain. CC, coiled-coil domain. N.D., not detected.
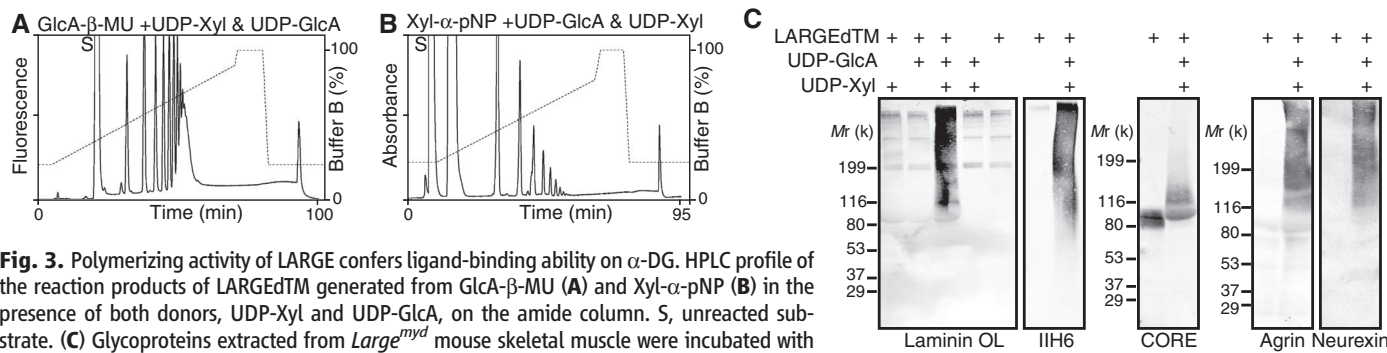

Fig. 3. Polymerizing activity of LARGE confers ligand-binding ability on α-DG. HPLC profile of the reaction products of LARGEdTM generated from GlcA-β-MU (**A**) and Xyl-α-pNP (**B**) in the presence of both donors, UDP-Xyl and UDP-GlcA, on the amide column. S, unreacted substrate. (**C**) Glycoproteins extracted from Large^{myd} mouse skeletal muscle were incubated with LARGEdTM, with or without UDP-GlcA and UDP-Xyl, and analyzed by immunoblotting with IIH6 or the CORE antibody, or by overlay assays (OLs) using laminin-G domain–containing ECM ligands (laminin, agrin, or neurexin).
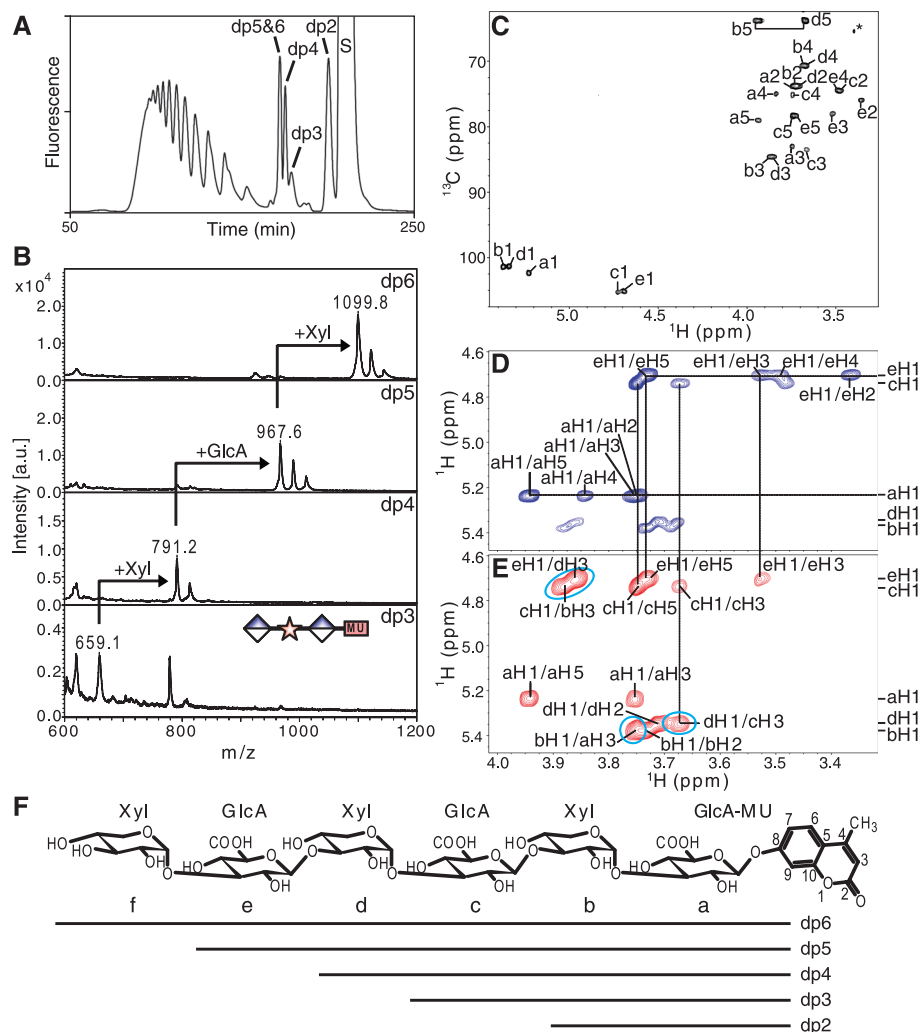
Fig. 4. MS and NMR analyses of products obtained from in vitro LARGE enzymatic reaction products, using GlcA-β-MU as the acceptor and UDP-GlcA and UDP-Xyl as the donors. (**A**) Separation profile of polymeric oligosaccharide by Superdex Peptide 10/300. S, unreacted substrate. (**B**) Matrix-assisted laser desorption–ionization tandem MS analysis of products dp3 to dp6. (**C**) HMQC spectrum of dp5 at 15°C. Assigned cross peaks are labeled with a letter representing the subunit [as designated in (F)], and a number representing the position on that subunit. The cross peak derived from sample impurities is marked by an asterisk. (**D**) TOCSY spectrum of dp5, collected with a mixing time of 120 ms at 15°C. (**E**) ROESY spectrum of dp5, collected with a mixing time of 300 ms at 15°C for the assignment of interglycosidic linkages (indicated by blue circles). The first letter in each label refers to the sugar subunit and the second to the hydrogen position of that subunit. (**F**) Structures of the polymeric oligosaccharides produced by the LARGE enzymatic reaction in vitro, with the sugar subunits labeled a to f.

tiple quantum coherence spectroscopy (HMQC), total correlation spectroscopy (TOCSY), and rotating-frame Overhauser effect spectroscopy (ROESY) spectra for dp5 are shown in Fig. 4, C to E, respectively. The majority of the spin systems of the sugar residues can be traced and assigned using different TOCSY mixing times together with double-quantum filtered correlated spectroscopy (COSY) spectra (Fig. 4D and fig. S11). GlcA residues c and e were linked via β1-3 linkages to Xyl residues b and d, respectively (Fig. 4E); and Xyl residues b and d were connected to GlcA residues a and c via α1-3 linkages, respectively (Fig. 4E). The structures of products dp2 to dp6 are shown in Fig. 4F; complete NMR assignments are listed in table S1. The fact that the glycosidic linkages were preserved among all tested products indicates that LARGE is a polymerizing enzyme with UDP-GlcA:αXyl β1,3-GlcA-T and UDP-Xyl:βGlcA α1,3-Xyl-T activities.

Here, we have identified the enzymatic function of LARGE, which produces a polysaccharide with repeating units of [-3Xyl-α1,3GlcAβ1-]. We believe that LARGE synthesizes the polymer on the O-mannosyl glycan of α-DG in vivo, but can possibly act on other glycans and/or other protein substrates when the enzyme concentration is artificially high. α-DG binds the LG4 and 5 domains of laminin alpha chains, and it is suggested that three basic patches contribute to these interactions (18). The LARGE-synthesized, negatively charged glycan on α-DG likely binds to laminin through electrostatic associations with these basic patches, a notion supported by the fact that one patch, 2719RKR contributes to binding with heparin, which contains acidic sugars GlcA and iduronic acid. The glycan we have observed resembles heparin-HS– and CS-DS–GAGs, linear polysaccharides that consist of repeating disaccharides and are synthesized by copolymerases with dual glycosyltransferase activities. Our findings may extend the types of GAG that provide a platform to retain molecules onto cell surface and/or in the ECM.

References and Notes
1. A. Varki et al., Eds., Essentials of Glycobiology (Cold Spring Harbor, New York, ed. 2, 2009).
2. O. Ibraghimov-Beskrovnaya et al., Nature 355, 696 (1992).
3. R. Barresi, K. P. Campbell, J. Cell Sci. 119, 199 (2006).
4. T. Yoshida-Moriguchi et al., Science 327, 88 (2010).
5. C. Longman et al., Hum. Mol. Genet. 12, 2853 (2003).
6. C. Godfrey, A. R. Foley, E. Clement, F. Muntoni, Curr. Opin. Genet. Dev. 21, 278 (2011).
7. M. Kanagawa et al., Cell 117, 953 (2004).
8. R. Barresi et al., Nat. Med. 10, 696 (2004).
9. J. M. Ervasti, K. P. Campbell, J. Cell Biol. 122, 809 (1993).
10. H. Yamada et al., J. Neurochem. 66, 1518 (1996).
11. H. Bakker et al., J. Biol. Chem. 284, 2576 (2009).
12. N. B. Schwartz, L. Galligani, P. L. Ho, A. Dorfman, Proc. Natl. Acad. Sci. U.S.A. 71, 4047 (1974).
13. P. M. Coutinho, E. Deleury, G. J. Davies, B. Henrissat, J. Mol. Biol. 328, 307 (2003).
14. M. Brockington et al., Hum. Mol. Genet. 14, 657 (2005).

(15), and anionic sugars distinct from sialic acid are involved (16). Thus, we tested whether LARGE could add Xyl and GlcA to the acceptor on α-DG, by performing the LARGEdTM reaction using both donors. Multiple products were generated for both acceptors (Xyl-α-pNP and GlcA-β-MU) (Fig. 3, A and B). We next asked whether this enzymatic activity could confer ligand-binding ability to α-DG in vitro, using skeletal muscle glycoproteins from the Large^myd mouse [in which a mutation in the LARGE gene causes defects in α-DG glycosylation (17)] as the acceptor substrate. Functional modification was robust only when both UDP-GlcA and UDP-Xyl were present (Fig. 3C). Thus, LARGE can assemble a polysaccharide with

ligand-binding activity onto the immature glycan of the Large^myd α-DG.

To identify the precise glycan structure that LARGE generates, we performed a large-scale enzymatic reaction with GlcA-β-MU, separated the products by gel filtration (Fig. 4A), and further purified those peaks (fig. S10). MS analysis of the product peaks ranging from a degree of polymerization (dp) of 3 to 6 showed m/z values corresponding to those of the products expected to be sequentially modified by GlcA and Xyl (Fig. 4B). Products dp2 to dp6 were further analyzed by nuclear magnetic resonance (NMR) to determine how the sugars are linked (fig. S11 to S15). Representative ^{13}C/^{1}H heteronuclear mul-

15. E. Hohenester, D. Tisi, J. F. Talts, R. Timpl, *Mol. Cell* **4**, 783 (1999).
16. A. C. Combs, J. M. Ervasti, *Biochem. J.* **390**, 303 (2005).
17. P. K. Grewal, P. J. Holzfeind, R. E. Bittner, J. E. Hewitt, *Nat. Genet.* **28**, 151 (2001).
18. D. Harrison et al., *J. Biol. Chem.* **282**, 11573 (2007).

RNA Elimination Machinery Targeting Meiotic mRNAs Promotes Facultative Heterochromatin Formation

Martin Zofall, Soichiro Yamanaka, Francisca E. Reyes-Turcu, Ke Zhang, Chanan Rubin,* Shiv I. S. Grewal†

Facultative heterochromatin that changes during cellular differentiation coordinates regulated gene expression, but its assembly is poorly understood. Here, we describe facultative heterochromatin islands in fission yeast and show that their formation at meiotic genes requires factors that eliminate meiotic messenger RNAs (mRNAs) during vegetative growth. Blocking production of meiotic mRNA or loss of RNA elimination factors, including Mmi1 and Red1 proteins, abolishes heterochromatin islands. RNA elimination machinery is enriched at meiotic loci and interacts with Clr4/SUV39h, a methyltransferase involved in heterochromatin assembly. Heterochromatin islands disassemble in response to nutritional signals that induce sexual differentiation. This process involves the antisilencing factor Epe1, the loss of which causes dramatic increase in heterochromatic loci. Our analyses uncover unexpected regulatory roles for mRNA-processing factors that assemble dynamic heterochromatin to modulate gene expression.

Heterochromatin assembly is critical for various chromosomal processes (*1–3*). In fission yeast (*Schizosaccharomyces pombe*), noncoding RNAs (ncRNAs) and RNA interference (RNAi) factors implicated in processing ncRNAs facilitate loading of Clr4/Suv39h to assemble constitutive heterochromatin domains (*4, 5*). Clr4 methylates histone H3 lysine 9 (H3K9me) to create binding sites for chromodomain proteins, including the Chp1 subunit of the Ago1-containing RNA-induced transcriptional gene silencing (RITS) complex, as well as HP1 family proteins Swi6 and Chp2, which associate with chromatin modifiers, including Snf2–histone deacetylase repressor complex (SHREC) involved in transcriptional silencing (*3*).

Apart from constitutive heterochromatin domains at centromeres, subtelomeres, and mating-type locus, H3K9me and HP1 proteins can also be detected within additional genomic regions at discrete genes in the *S. pombe* genome (*6*). However, the assembly of heterochromatin targeting genes and its modifications in response to signals that modulate gene expression have not been explored. To address this, we mapped H3K9me across the genome (*7*).

Laboratory of Biochemistry and Molecular Biology, National Cancer Institute, National Institutes of Health, Bethesda, MD 20892, USA.

*Present address: Evogene, Rehovot, Israel.
†To whom correspondence should be addressed. E-mail: grewals@mail.nih.gov

Besides previously reported heterochromatin loci, we reproducibly detected H3K9me at several additional sites (Fig. 1A). These heterochromatin islands encompass ~30 loci, which include genes located adjacent to ncRNAs and a few long terminal repeats (Fig. 1B). Overlapping transcription at convergent genes is believed to target H3K9me via RNAi (*8*), whereas heterochromatin islands correspond to both convergent and nonconvergent loci (Fig. 1, B and C). A distinctive feature of heterochromatin islands is their preferential association with meiotic genes, which are silenced during vegetative growth (table S1). Most H3K9me enrichment corresponds to either open reading frames or 3′ ends of genes (Fig. 1B), consistent with transcription-coupled processes targeting H3K9me. Histone H3K4 methylation, a modification linked to RNA polymerase II transcription, could be detected at the 5′ ends of genes within heterochromatin islands (fig. S1).

Factors that bind H3K9me and their associated effectors localize to heterochromatin islands: Chromatin immunoprecipitation (ChIP) detected the Clr4 complex (ClrC) subunit Raf2, Swi6/HP1, as well as posttranscriptional and transcriptional silencing activities, such as RNAi effector complex RITS (Chp1 and Ago1) and SHREC (Clr3 and Mit1), respectively, at heterochromatin islands (fig. S2). Additionally, Dcr1 localizes to three genes corresponding to islands (*9*). We also found the cohesin-loading factor Mis4, which interacts with Swi6/HP1 (*10*), and the cohesin subunit Rad21 enriched at meiotic heterochromatin islands (fig. S2).

Our analysis identified the antisilencing factor Epe1 (*11, 12*) at heterochromatin islands (fig. S2). The loss of Epe1 caused the spread of H3K9me at most heterochromatin islands and at subtelomeric regions (fig. S3, A and B). Moreover, *epe1Δ* cells showed several H3K9me peaks that were not detected in wild-type cells (fig. S3C). More than 30 additional peaks mapped to ~100 convergent and nonconvergent loci. As in the case of the wild type, a major fraction of heterochromatin islands in *epe1Δ* mapped to meiotic genes. Thus, the *S. pombe* genome appears to harbor numerous heterochromatin nucleation sites, but heterochromatin assembly at many of these loci is suppressed by factors such as Epe1.

Given that heterochromatin islands map to transcribed regions, we wondered if RNAi targets heterochromatin to these loci. The loss of Dicer (Dcr1) or Argonaute (Ago1) caused only partial or no reduction in H3K9me at heterochromatin islands except island 5, which showed considerable reduction of H3K9me (fig. S4, A and B). Moreover, de novo targeting of H3K9me to *ssm4* and *mei4* occurred even in the absence of Ago1, albeit at levels lower than those of the wild type (fig. S4C), suggesting that additional RNAi-independent mechanism(s) target heterochromatin to meiotic loci. We also investigated the effects of histone deacetylases (HDACs), including Sir2 and SHREC (*3*), implicated in heterochromatin formation. Deletion of *sir2* encoding a nicotinamide adenine dinucleotide–dependent HDAC (*3*) caused defective H3K9me at the majority of islands (fig. S5A), but SHREC subunits were dispensable (fig. S5B).

We next sought to investigate the mechanism of heterochromatin assembly at meiotic loci. Meiotic genes such as *ssm4* are transcribed during vegetative growth, but their transcripts are processed by the exosome (*13–16*). The loss of Rrp6, an exosome-associated 3′-to-5′ exonuclease (*17*), led to the accumulation of *ssm4* mRNA and a long RNA, which initiated from a promoter upstream of *tpr1* (Fig. 2A and fig. S6). When production of *ssm4* mRNA and the long RNA was disrupted by insertion of *ura4* transcription terminator at the *ssm4* promoter (Fig. 2A), the resulting strain showed the loss of H3K9me at the *ssm4* (Fig. 2B). We also generated a strain in which *ura4* terminator specifically blocks long RNA, without affecting *ssm4* mRNA (fig. S7). *ssm4* mRNA was sufficient to nucleate heterochromatin, as disruption of the long RNA did not abolish H3K9me (fig. S7). Based on these data,

Supporting Online Material for

Dystroglycan Function Requires Xylosyl- and Glucuronyltransferase Activities of LARGE

Kei-ichiro Inamori, Takako Yoshida-Moriguchi, Yuji Hara, Mary E. Anderson, Liping Yu, Kevin P. Campbell*

*To whom correspondence should be addressed. E-mail: kevin-campbell@uiowa.edu

This PDF file includes

Materials and Methods
SOM Text
Figs. S1 to S15
Table S1
References

Materials and Methods

<u>cDNAs</u>
The full-length LARGE expression vector has been described elsewhere (7, 19). Human UXS1 (NM_025076.3, pCMV6 vector, Myc-DDK-tagged) was purchased from Origene.

<u>LARGEdTM constructs and establishment of stable cell lines</u>

LARGEdTM
The construct expressing LARGE without its transmembrane region was generated by amplifying cDNA fragments of human LARGE from pIRES-puro3 LARGE-myc (19) using primer pairs (#7217: 5'-GAACGCGGCCGCTTTCGAAGATGGAAAGCCCG- 3' and #2998: 5'-TTGGCAGGAAGAGTCTTGGT-3' to produce the left fragment; and #3000: 5'-AAGTTTCCTGGATCCCCAAT-3' and #4112: 5'-TTGAATTCTAATGGTGATGGTGATGGTGGCTGTTGTTCTCGGCTGTGAG -3' to produce the right fragment). The left fragment was digested with NotI and BamHI, and the right fragment with BamHI and EcoRI. The latter was then subcloned into the pcDNA3 vector (Invitrogen), after which the resulting plasmid was digested with BamHI and XbaI (whose recognition site is located at the 3'-region of the EcoRI site). The two fragments were then ligated into a NotI/XbaI-digested p3xFLAG-CMV-9 vector (Sigma-Aldrich) to generate construct p3xFLAG-CMV-9-LARGEdTM, which expresses a LARGE fusion protein (amino acids 34-756) tagged with a 3xFLAG at its N-terminus and Hisx6 at its C-terminus.

LARGEdTM DXD1
The construct harboring the DXD1 (D242N/D244N) mutations was generated by digesting p3xFLAG-CMV-9-LARGEdTM with EcoRI and XhoI, then treating it with T4 DNA polymerase (NEB) and allowing self-ligation. This strategy resulted in elimination of the EcoRV and NotI recognition sites derived from pcDNA3, in the construct p3xFLAG-CMV-9-LARGEdTM-delta. A DNA fragment harboring the DXD1 (D242N/D244N) mutations was amplified using 5'-phosphorylated primers (#3848: 5'-ATGGGCGTGGATAGCGGTTTGACTC-3' and #7604: 5'-ATTCGTGTTAAGGACGATGACTCTCTCCAG-3'), digesting the product with NotI, and then ligating it into NotI/EcoRV-digested p3xFLAG-CMV-9-LARGEdTM-delta vector to produce p3xFLAG-CMV-9-LARGEdTM-DXD1.

LARGEdTM DXD3
The construct harboring the DXD3 (D563N/D565N) mutations was generated using two-sided splicing involving overlapping extension. The left and right fragments were amplified using the primer pairs (#3000: 5'-AAGTTTCCTGGATCCCCAAT-3' and #7602: 5'-CATGGGCAGGAAGTTAATGTTAGACAGGAACAT-3' to generate the left fragment; and #7601: 5'-ATGTTCCTGTCTAACATTAACTTCCTGCCCATG-3' and #2999: 5'-CCTTTCGTCCAGACGTGGTA-3' to generate the right fragment). These PCR products were used as templates for a subsequent amplification using primers #3000 and #2999. The resulting band was digested with KpnI and cloned into KpnI-digested p3xFLAG-CMV-9-LARGEdTM vector to produce p3xFLAG-CMV-9-LARGEdTM-DXD3.

Generation of cell lines stably expressing LARGEdTM proteins
HEK293 cells were transfected with constructs p3xFLAG-CMV-9-LARGEdTM-WT, DXD1, and DXD3 (each of which contains a neomycin resistance cassette), using FuGENE 6 (Roche Applied Science), and selected in medium containing Geneticin (500 μg/ml, Invitrogen). Single colonies were isolated and analyzed for expression of the respective LARGEdTM protein, by immunoblotting with anti-FLAG M2 antibody (Sigma-Aldrich). The stable clones obtained in this way were adapted to serum-free medium 293SFMII (Invitrogen) and cultivated in CELLine bioreactors (CL1000, Argos Technologies).

Antibodies
Antibodies to α-DG glycan (IIH6) and core (goat20 or sheep5) epitopes have been described previously (4, 20). Anti-β-DG antibody 7D11 and anti-HS antibody 10E4 were purchased from Developmental Studies Hybridoma Bank at University of Iowa and from US Biological, respectively.

Glycoprotein enrichment, immunoblotting, and ligand overlays
Glycoprotein enrichment by wheat germ agglutinin (WGA)-agarose beads, immunoblotting, and ligand overlays were performed as described previously (20).

Compositional sugar analysis by GC-MS
Recombinant α-DG produced in HEK293 cells (21) was purified using agarose-bound Jacalin (Vector Laboratories) according to the manufacturer's instructions. The bound α-DG was eluted with 800 mM galactose and then desalted extensively. The purified α-DG was treated with PNGaseF, *O*-glycosidase, and α-2(3,6,8,9) neuraminidase, using the Enzymatic Protein Deglycosylation Kit (Sigma-Aldrich) according to manufacturer's protocol. Gas chromatography-mass spectrometry (GC-MS) analysis of trimethylsilyl derivatives was conducted by the Glycotechnology Core Resource (UCSD).

Xyloside treatment
Nearly confluent LARGE-expressing CHO cells were trypsinized and replated at a 1:5 dilution in fresh medium containing 1 mM Xyl-α-pNP (Calbiochem), and then cultured for 2 days.

Purification of LARGEdTM
LARGEdTM secreted into the culture medium by HEK293 cells was purified using the Talon metal affinity resin (Clontech) according to the manufacturer's instruction. The purity of the protein was confirmed by SDS-PAGE and Coomassie Brilliant Blue staining. The eluate was desalted for enzyme assay, using an Amicon Ultra-4 centrifugal filter unit (Millipore).

Analysis of LARGE enzymatic activity
The HPLC-based enzyme assay for LARGEdTM was performed using either Xyl-α-pNP or GlcA-β-MU (Sigma-Aldrich) as the acceptor. The sample was incubated for 1 or 2 h at 37ºC, with 5 mM UDP-GlcA or 0.5 mM UDP-Xyl and in 0.1 M 3-(N-morpholino)propanesulfonic acid (MOPS) buffer, pH 7.5, at 10 mM $MnCl_2$, 10 mM

MgCl$_2$, and 0.5% Triton X-100. The reaction was terminated by boiling for 5 min, and the supernatant was analyzed for (a) product, using a 4.6 x 250 mm GlycoSep N column (ProZyme), and (b) enzymatic activity, using a 4.6 x 250 mm Supelcosil LC-18 column (Supelco). For the GlycoSep N column, solvent A was acetonitrile, and solvent B was 250 mM ammonium formate, pH 4.4. For the LC-18 column, solvent A was 50 mM ammonium formate, pH 4.0, and solvent B was 80% acetonitrile in solvent A. The elution of pNP derivative and MU derivative was monitored by absorbance at 300 nm and by a fluorescence detector set at 325 nm for excitation and at 380 nm for emission, respectively. The enzymatic activity was examined in triplicate, and calculated as the peak area of the product.

In vitro LARGE enzymatic reaction using *LARGE^{myd}* mouse skeletal muscle
WGA-enriched glycoproteins from *LARGE^{myd}* mouse skeletal muscle were incubated overnight at 37ºC with LARGEdTM and 10 mM UDP-GlcA plus 10mM UDP-Xyl, in 0.1 M MOPS, pH 7.5, at 10 mM MgCl$_2$ and 0.5% Triton X-100. The reaction product was subjected to immunoblotting or ligand overlay.

Separation and purification of products of LARGE-catalyzed reaction
A large-scale reaction was carried out with 10 mM each of UDP-GlcA and UDP-Xyl, at 37ºC for 7 h, and the sample was separated by running it over two Superdex Peptide 10/300 gel-filtration columns (GE Healthcare) in tandem, using isocratic elution with 50 mM ammonium bicarbonate at a flow rate of 0.15 ml/min. The collected peak samples were lyophilized and dissolved in 50 mM ammonium formate, pH 4.0 and further purified over an LC-18 column.

LTQ XL liner ion trap MS and HPAEC-PAD analyses
The glycan samples were dissolved in 50% acetonitrile/water (v/v) and directly infused into an LTQ XL liner ion-trap mass spectrometer (Thermo Scientific, Inc.) at 5 µl/min, using a syringe pump. The samples were ionized using negative nanospray ionization. Capillary temperature and needle voltage were 200°C and -4.5-5 kV, respectively. Collisions for MS^n were carried out with an isolation window of 3.0 u and a normalized collision energy of 20-35%.

MALDI-TOF MS/MS
α-cyano-4-hydroxycinnamic acid (saturated in a mixture of acetonitrile and 0.1% TFA in 1:1 v/v) was used as the matrix. Mass spectra were obtained using a Bruker ultrafleXtreme MALDI-TOF/TOF mass spectrometer in negative linear mode. MALDI targets were prepared by spotting 1.0 µl of a mixture of the sample and the matrix (1:1 v/v ratio) onto an MTP anchorchip 800/384 plate (Bruker). Angiotensin I and a peptide of molecular weight 1500 kD, were used as external standards. MS/MS spectra were obtained in LIFT mode.

NMR study
After hydroxyl hydrogens of the sample fractionated by gel filtration and LC-18 chromatographies were replaced with deuterium (repeated dissolving of the sample in 99.9% D$_2$O followed by lyophilisation), the samples were dissolved in 10 mM NaPO$_4$

buffer, pH 6.5, in 100% D_2O and used for the NMR studies. ^1H homonuclear two-dimensional DQF-COSY, TOCSY (fig. S11), and ROESY experiments, and $^1H/^{13}C$ heteronuclear two-dimensional HMQC and HMBC experiments were carried out using a Bruker Avance II 800 MHz spectrometer equipped with a cryoprobe. NMR spectra were processed using the NMRPipe package, and analyzed using NMRView.

Flow cytometry
CHO, pgsI-208, pgsA-745 cells (22) or xyloside-treated cells were analyzed by flow cytometry using IIH6, CORE (goat20), or 10E4, as described previously (4).
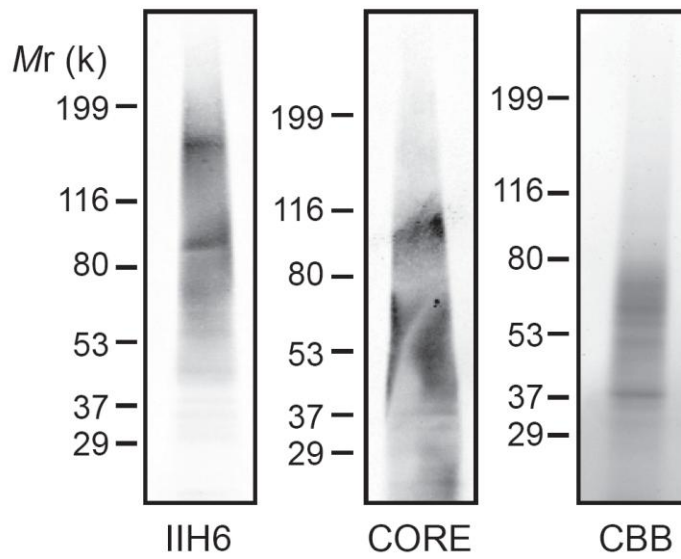
Fig. S1.

HEK293 cells stably expressing both α-DG and LARGE produce functionally modified recombinant α-DG. Recombinant α-DG secreted into the serum-free medium was purified using agarose-bound Jacalin. The eluate was subjected to immunoblotting with the IIH6 and CORE antibodies. CBB, Coomassie Brilliant Blue staining.
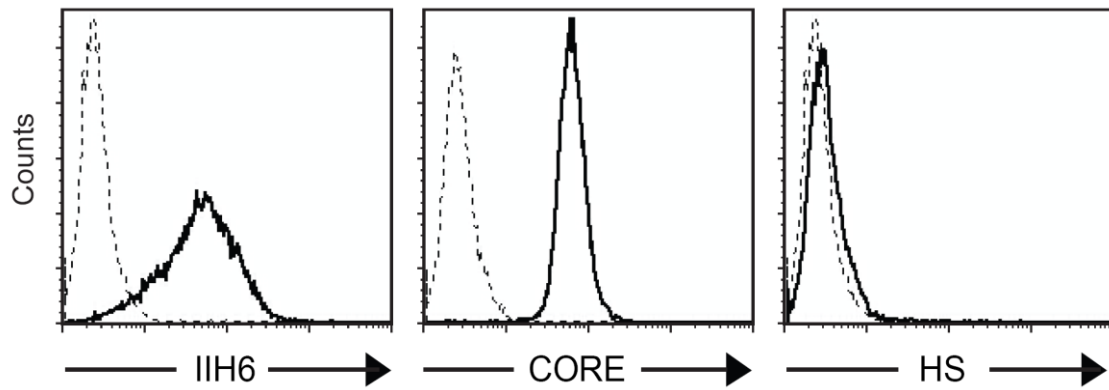
Fig. S2.

GAG-deficient CHO mutant pgsA-745 cells retain the ability to functionally modify α-DG. Cells were stained with the IIH6, CORE, or HS antibody, and then analyzed by flow cytometry. Dashed line, secondary antibody alone.
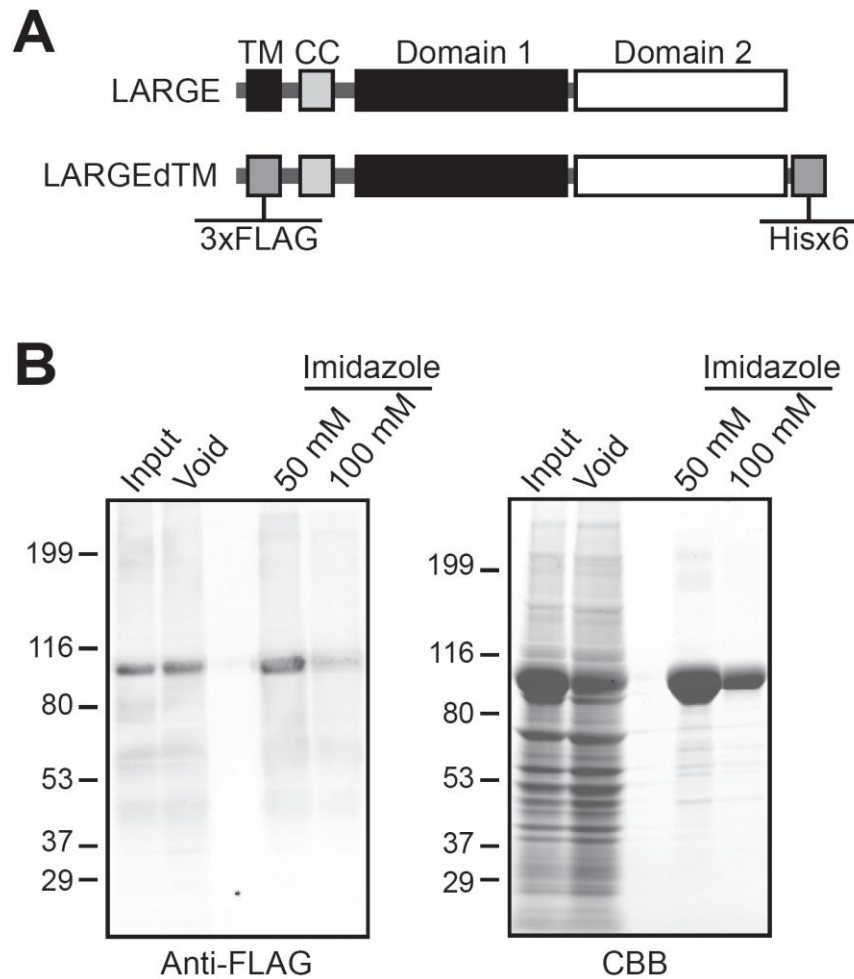
Fig. S3.
Purification of LARGEdTM. (A) Schematic representation of the LARGEdTM construct used in the LARGE enzymatic activity assay. The transmembrane (TM) sequence was replaced with a 3xFLAG tag sequence and the C-terminus was modified with a Hisx6 tag. CC, Coiled-coil domain. (B) The recombinant protein expressed in the culture medium was purified on a Talon metal affinity resin, and the eluates were analyzed by immunoblotting with anti-FLAG antibody. CBB, Coomassie Brilliant Blue staining.
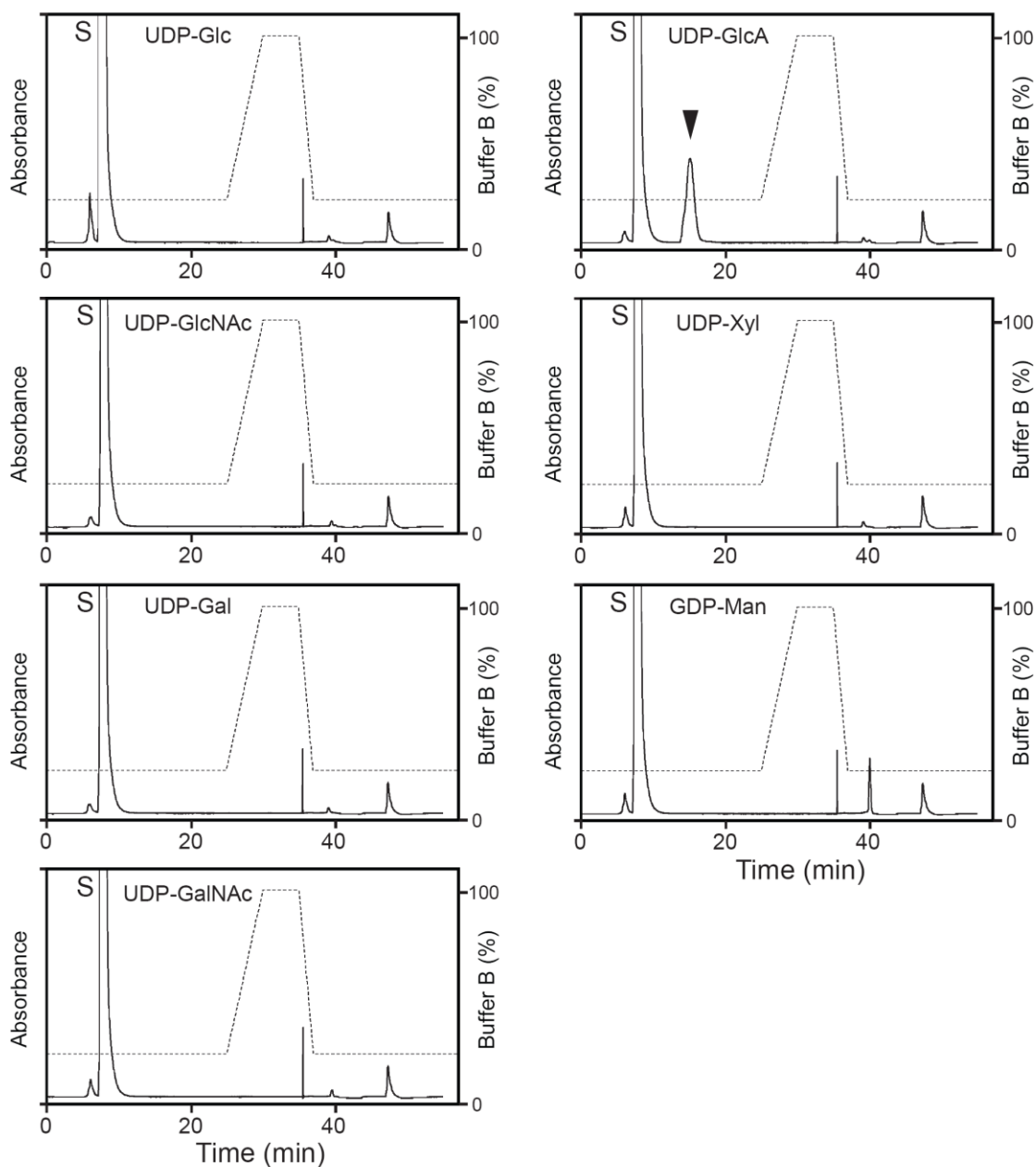
Fig. S4.

HPLC elution profile of the product of the LARGEdTM-catalyzed reaction when Xyl-α-pNP served as the acceptor. Xyl-α-pNP was incubated with LARGEdTM and the donor sugar indicated in panel, and the reaction product was analyzed by HPLC using a GlycoSep N column (solid line). S, unreacted substrate. Arrowhead indicates a unique peak observed only in the presence of UDP-GlcA. Dashed line, %B buffer.
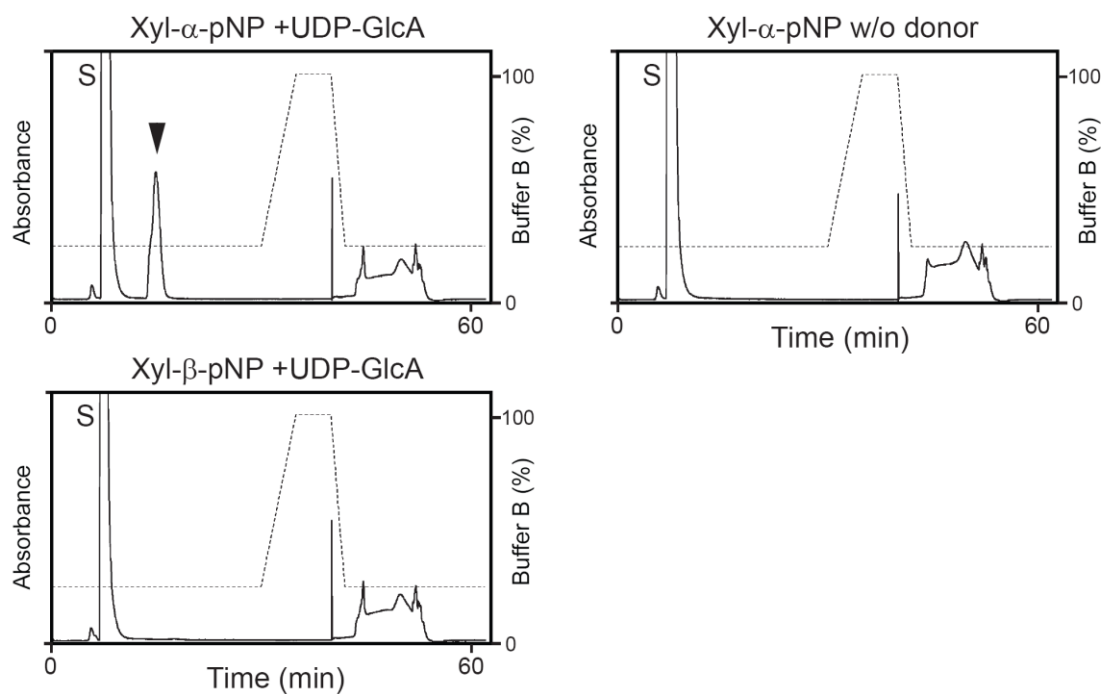
Fig. S5.

HPLC elution profile of the product of the LARGEdTM-catalyzed reaction when Xyl-α-pNP or Xyl-β-pNP served as the acceptor. Each Xyl-pNP form was incubated with LARGEdTM and UDP-GlcA, and the reaction product was analyzed by HPLC using a GlycoSep N column (solid line). S, unreacted substrate. Arrowhead indicates a unique peak observed only when Xyl-α-pNP serves as the acceptor, and UDP-GlcA is present. Dashed line, %B buffer.
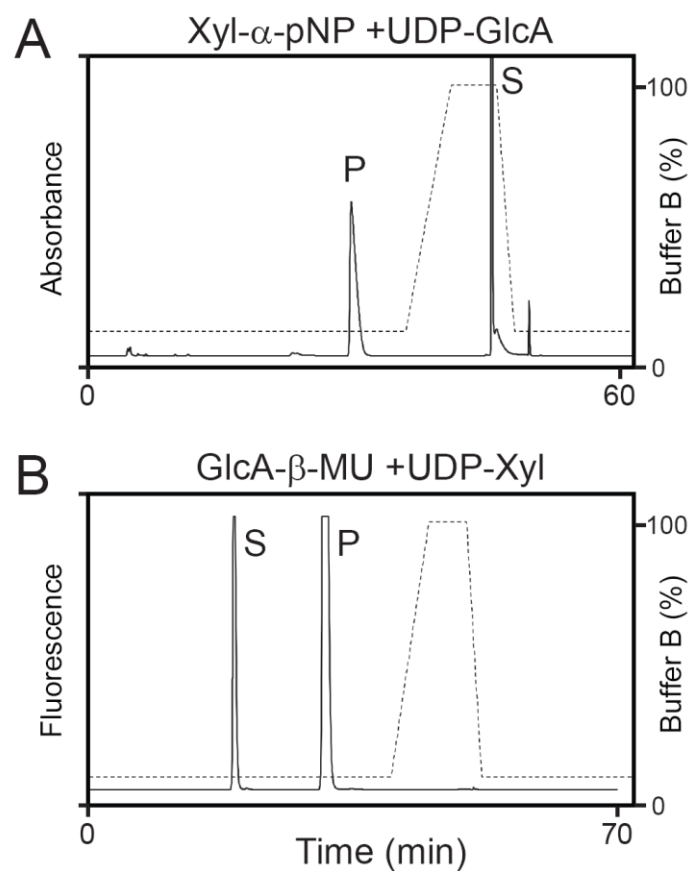
Fig. S6.

Isolation of the LARGEdTM-catalyzed reaction products for MS analysis. Product from Xyl-α-pNP (A) or GlcA-β-MU (B) was separated on an LC-18 column. Elution of the derivatives of pNP and MU was monitored by measuring absorbance at 300 nm (solid line in A) and fluorescence (solid line in B, detector set at 325 nm for excitation and 380 nm for emission), respectively. Dashed line, %B buffer. S, unreacted substrate. P, enzymatic product.
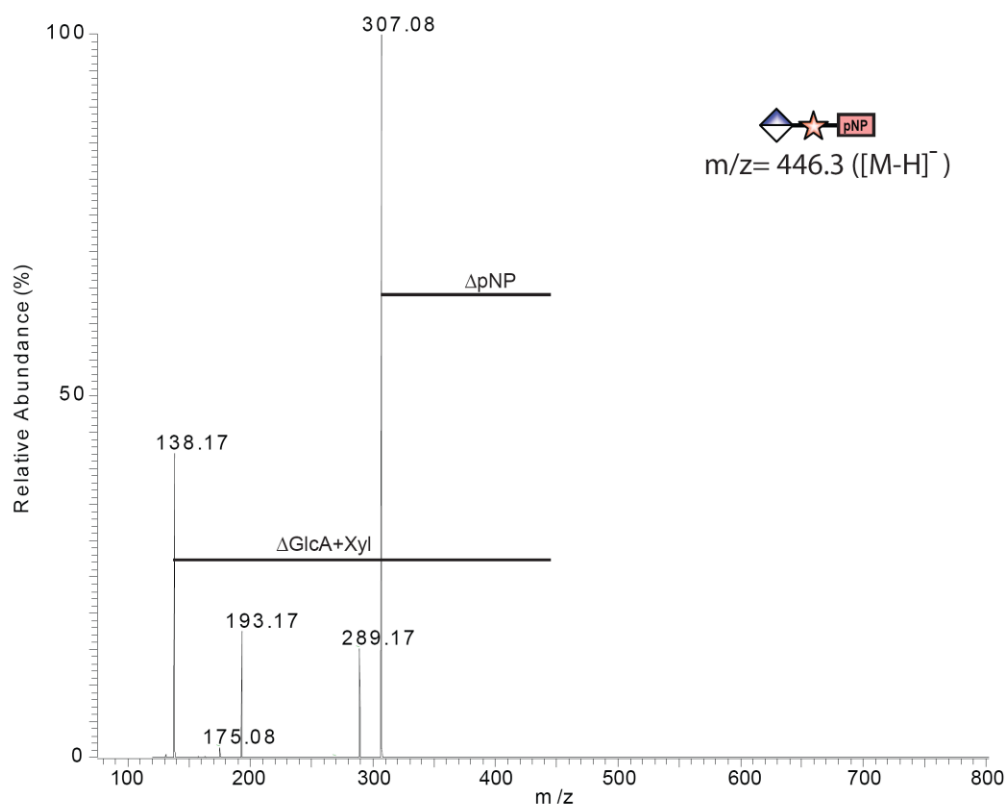
Fig. S7.
Nanospray ionization-linear ion-trap mass spectrometry in negative-ion mode. CID MS/MS spectrum derived from the parent ion [M-H]- (m/z 446.3). Star and diamond indicate Xyl and GlcA, respectively.
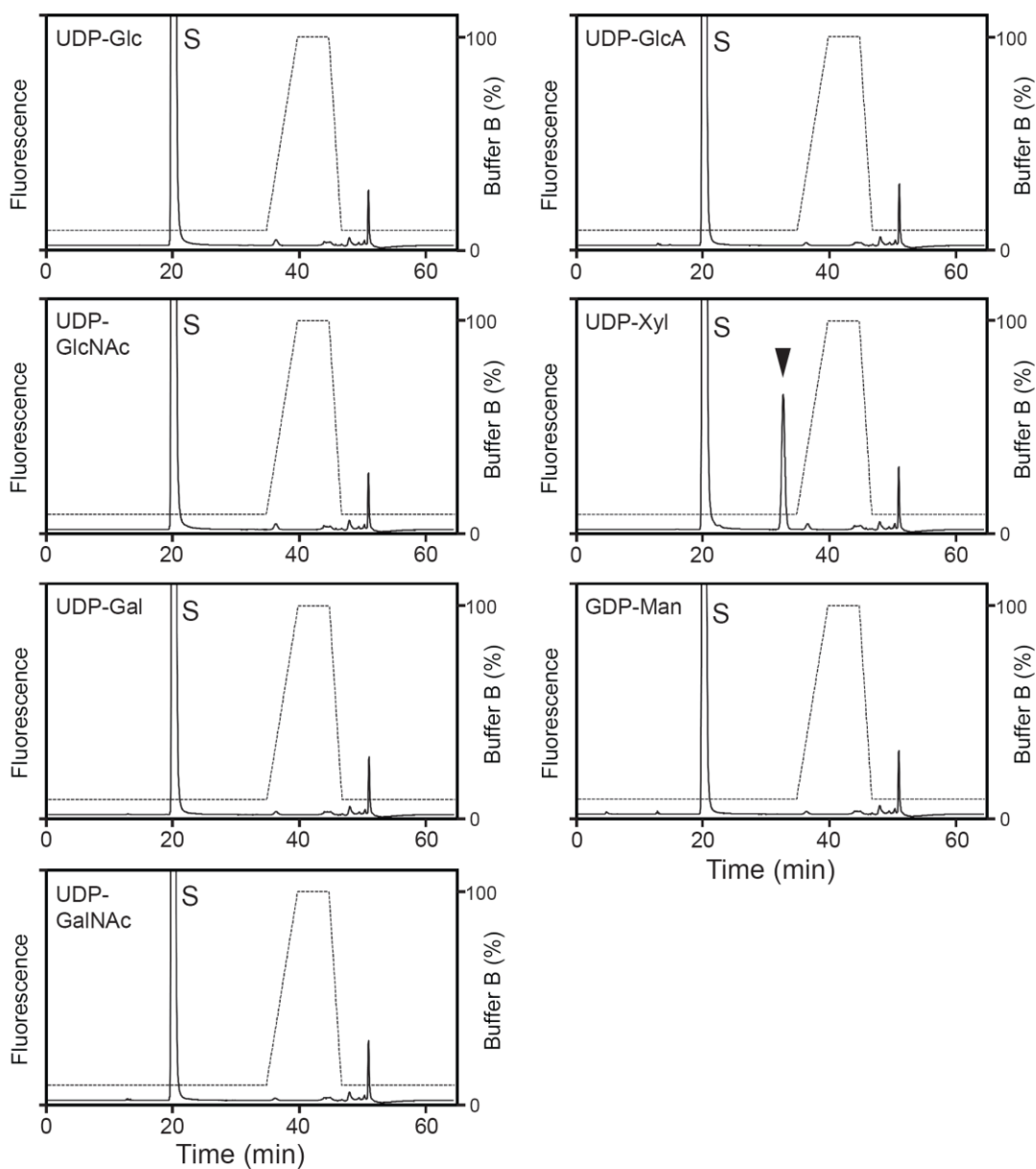
Fig. S8.

HPLC elution profile of the product of the LARGEdTM-catalyzed reaction when MU-β-GlcA served as the acceptor. MU-β-GlcA was incubated with LARGEdTM and the donor sugar indicated in panel, and the reaction product was analyzed by HPLC using an LC-18 column (solid line). S, unreacted substrate. Arrowhead indicates a unique peak observed only in the presence of UDP-Xyl. Dashed line, %B buffer.
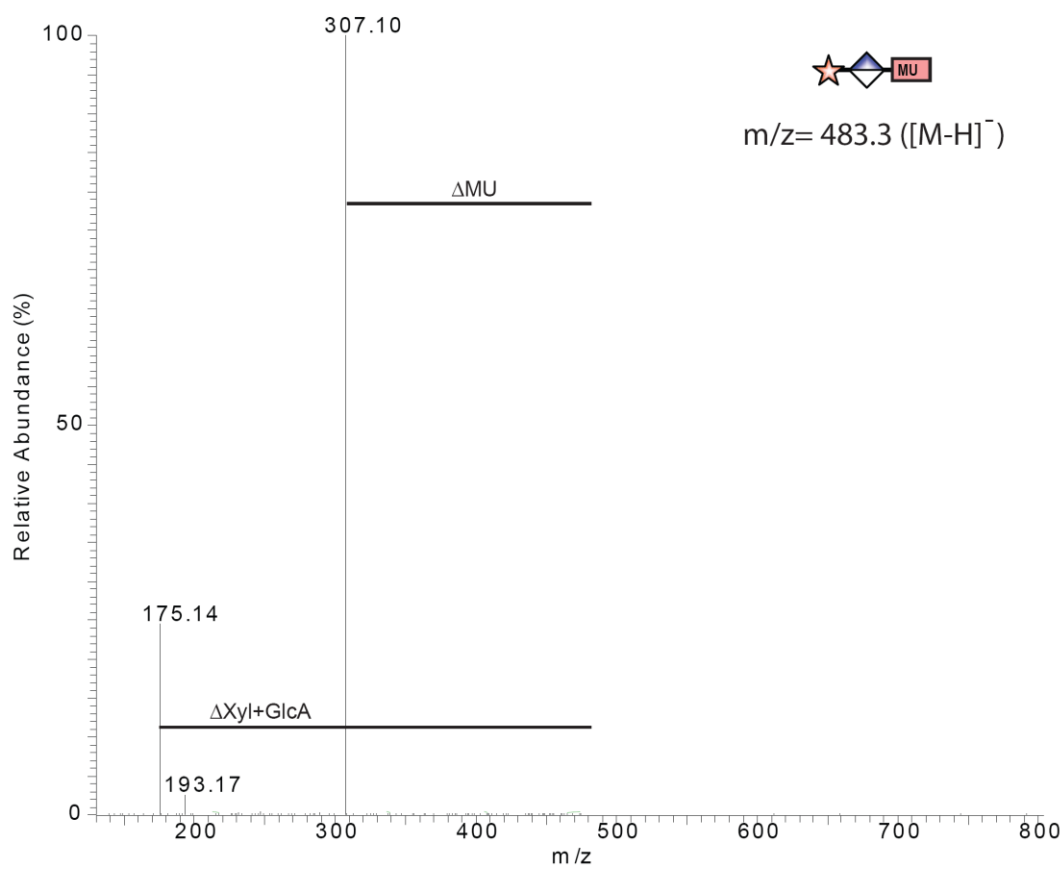
Fig. S9.

Nanospray ionization-linear ion trap mass spectrometry in negative ion mode. CID MS/MS spectrum derived from the parent ion [M-H]- (m/z 483.3). Star and diamond indicate Xyl and GlcA, respectively.
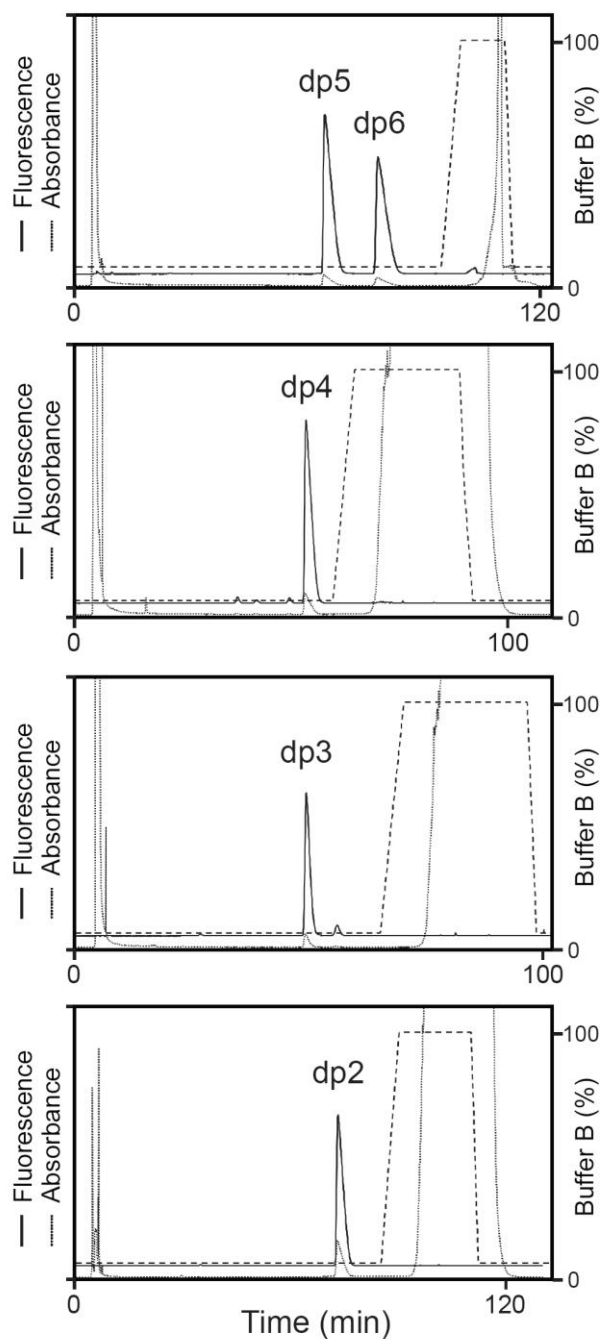
Fig. S10.

Purification of MU-β-GlcA derivatives by reversed-phase HPLC. Each peak isolated by gel-filtration (Fig. 4A) was further purified on an LC-18 column. Elution of the MU derivatives was monitored using a fluorescence detector set at 325 nm for excitation and 380 nm for emission (solid line). Dotted line, absorbance at 254 nm. Dashed line, %B buffer.
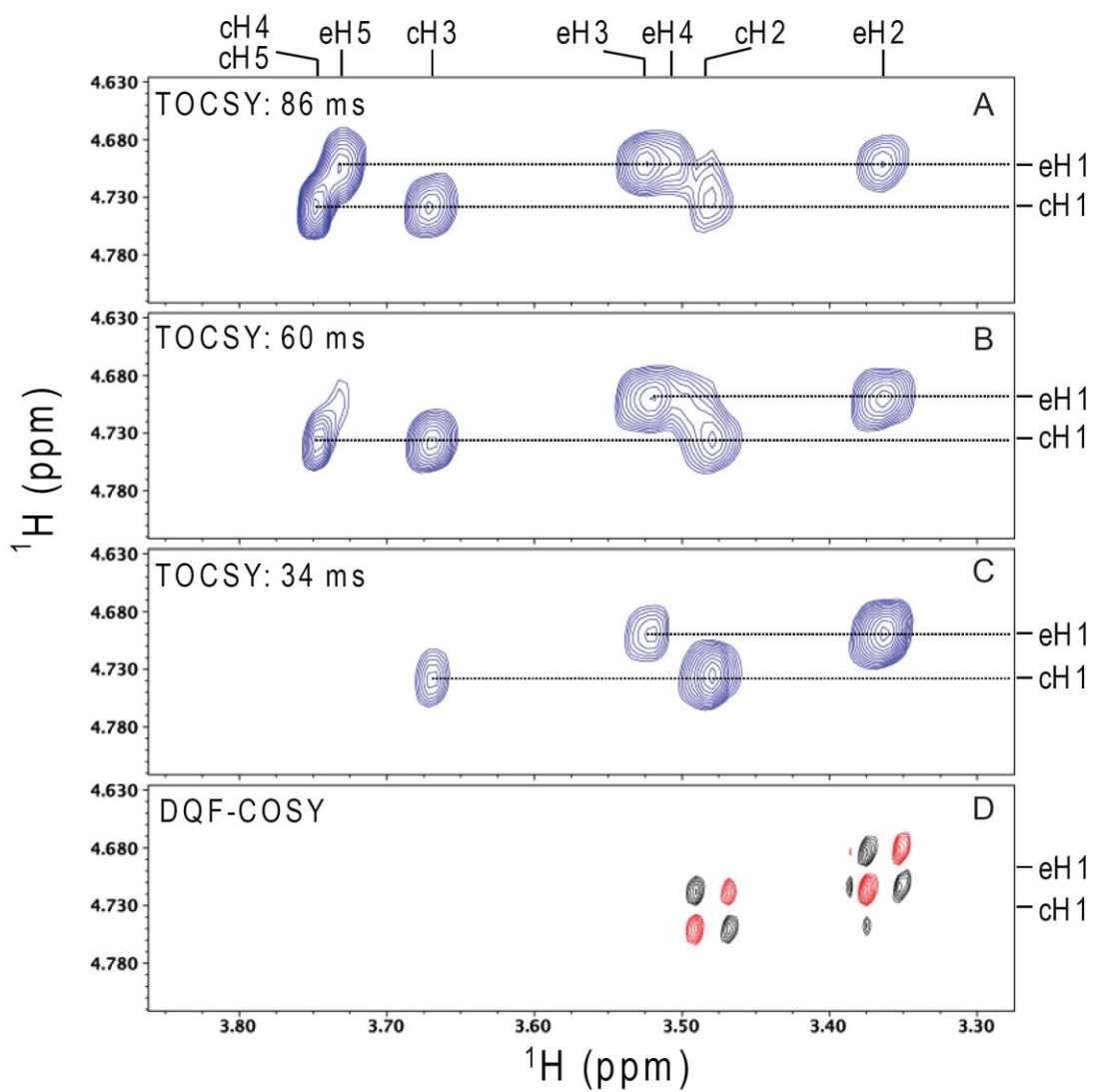
Fig. S11.

NMR analysis of dp5 at 15°C. TOCSY (A-C) and DQF-COSY (D) spectra for the assignment of proton in subunit c and e. The assigned protons are indicated along the top and right sides of the panels. TOCSY mixing times of 34, 60, and 86 ms were used for spectra C, B, and A, respectively.
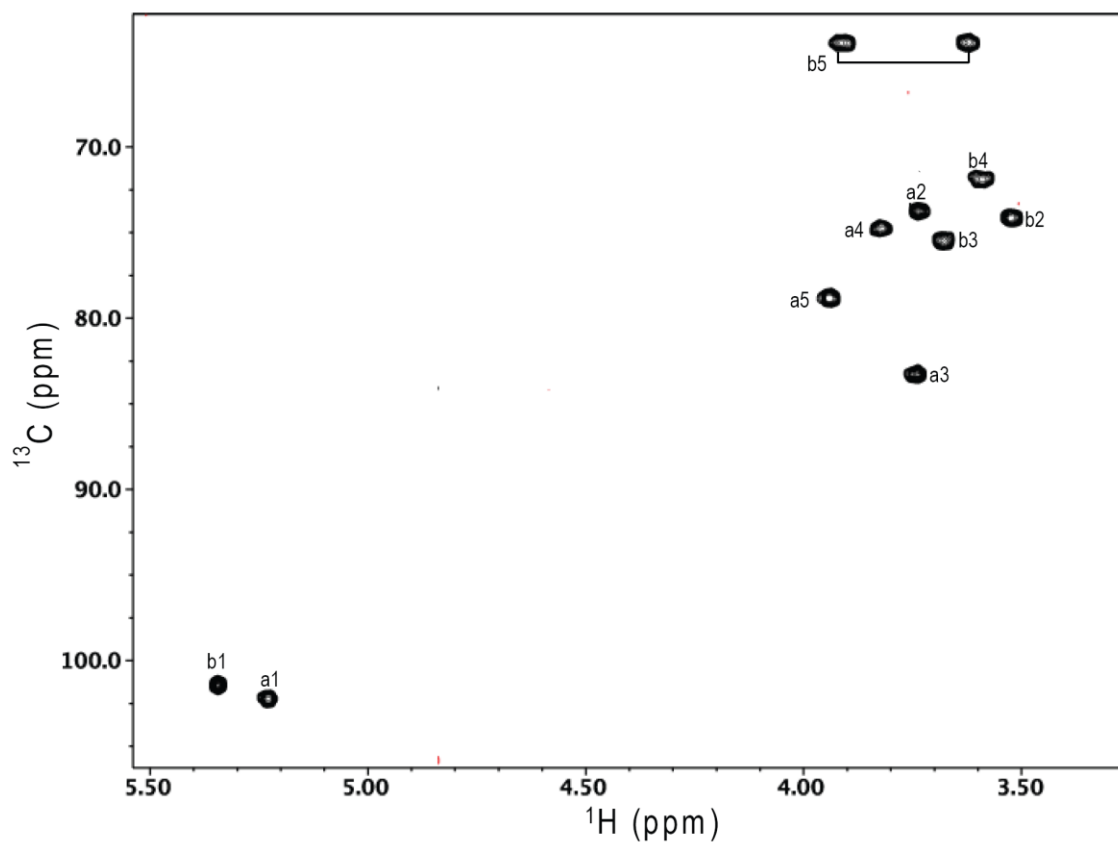
Fig. S12.

NMR analysis of product dp2 at 15ºC. HMQC spectrum, with the assigned cross peaks labeled with a letter indicating the subunit as designated in Fig. 4F, and a number indicating the position on that subunit.
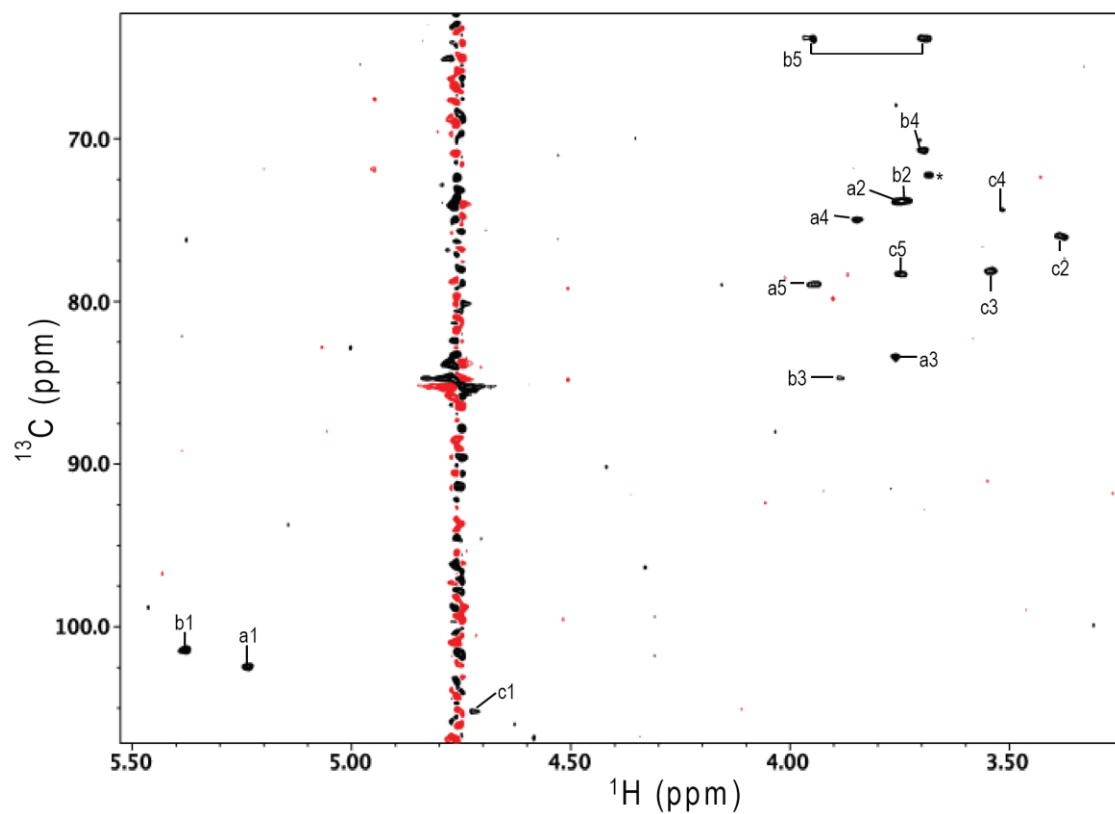
Fig. S13.

NMR analysis of product dp3 at 25ºC. Shown is the HMQC spectrum, with the assigned cross peaks labeled with a letter indicating the subunit as designated in Fig. 4F, and a number indicating the position on that subunit. The cross peak derived from sample impurities is indicated by an asterisk.

Fig. S14.

NMR analysis of product dp4 at 15°C. Shown is the HMQC spectrum, with the assigned cross peaks labeled with a letter indicating the subunit designated in Fig. 4F, and a number indicating the position on that subunit.

Fig. S15.

NMR analysis of product dp6 at 15ºC. Shown is the HMQC spectrum, with the assigned cross peaks labeled with a letter indicating the subunit designated in Fig. 4F, and a number indicating the position on that subunit.
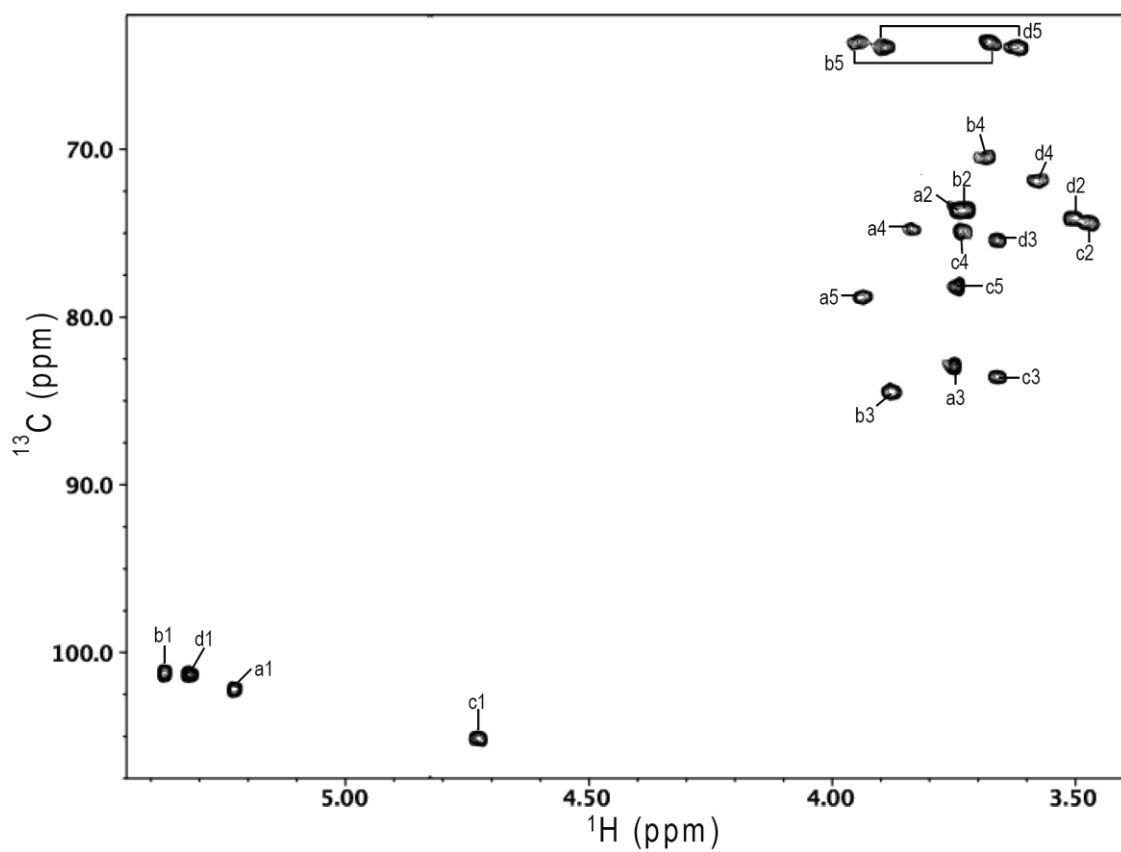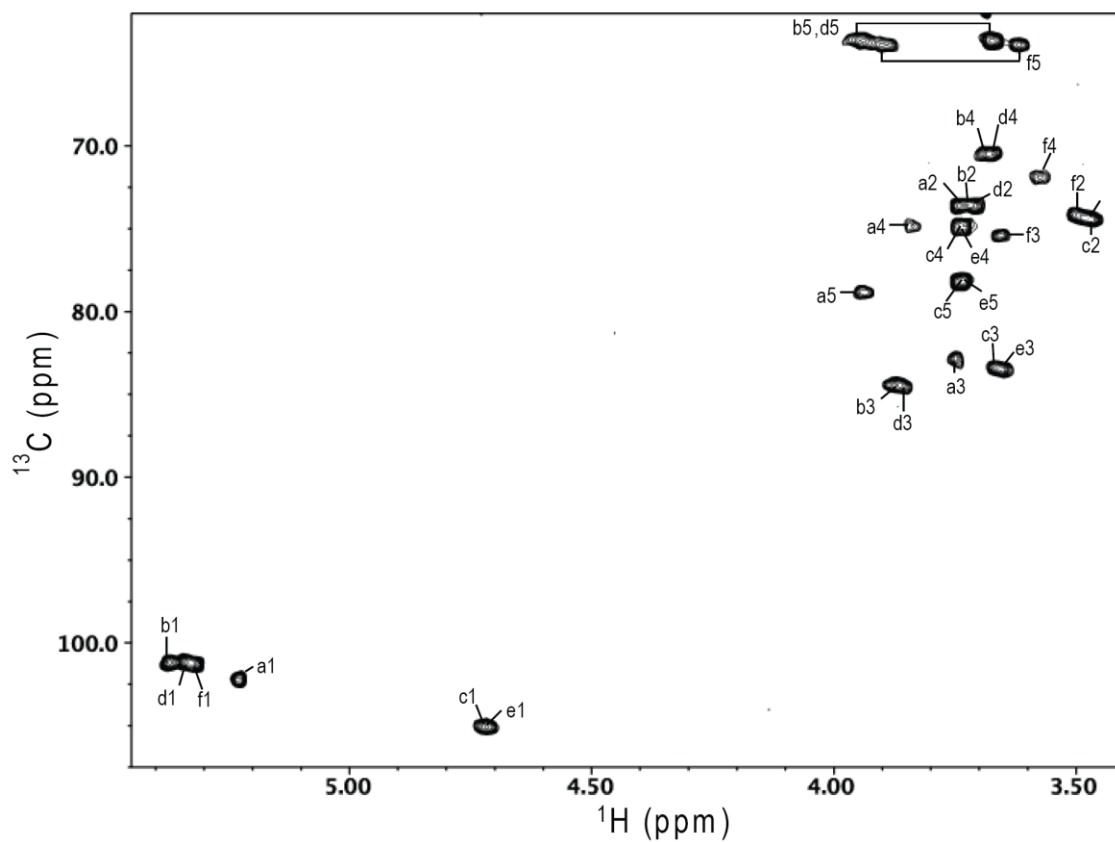
Table S1. Chemical shifts (ppm) of the signals in the ^{1}H and ^{13}C NMR spectra of some of the enzymatic reaction products of the glycosyltransferase LARGE.

Products	Sugar						Aromatic Ring[b]				
	1	2	3	4	5	6[b]	3	4-CH₃	6	7	9
dp2 (2 sugar units)											
→3)-β-D-GlcA-MU	5.24	3.76	3.76	3.84	3.95	-	6.28	2.47	7.76	7.13	7.13
a	102.6	74.1	83.9	75.0	78.9	177.7	113.9	20.7	129.3	116.3	106.4
α-D-Xyl-(1→	5.36	3.55	3.70	3.61	3.65, 3.91						
b	101.7	74.5	75.8	72.2	64.3						
dp3 (3 sugar units)											
→3)-β-D-GlcA-MU	5.23	3.76	3.76	3.85	3.95	-	6.30	2.47	7.78	7.16	7.15
a	102.4	73.9	83.4	75.0	79.0	177.7	114.1	20.7	129.5	116.7	106.8
→3)-α-D-Xyl-(1→	5.38	3.74	3.88	3.70	3.69, 3.95						
b	101.4	73.9	84.7	70.7	63.9						
β-D-GlcA-(1→	4.72	3.38	3.54	3.51	3.75						
c	105.2	76.0	78.1	74.4	78.3						
dp4 (4 sugar units)											
→3)-β-D-GlcA-MU	5.23	3.75	3.75	3.84	3.94	-	6.28	2.46	7.76	7.13	7.13
a	102.2	73.7	82.9	74.7	78.9	177.7	113.9	20.5	129.2	116.3	106.4
→3)-α-D-Xyl-(1→	5.37	3.73	3.88	3.68	3.68, 3.95						
b	101.2	73.7	84.5	70.5	63.6						
→3)-β-D-GlcA-(1→	4.72	3.48	3.66	3.74	3.74						
c	105.1	74.4	83.6	74.9	78.2						
α-D-Xyl-(1→	5.32	3.50	3.66	3.58	3.62, 3.89						
d	101.3	74.1	75.5	71.9	64.0						
dp5 (5 sugar units)											
→3)-β-D-GlcA-MU	5.23	3.75	3.75	3.84	3.94	-	6.28	2.46	7.76	7.13	7.13
a	102.2	73.6	83.0	74.7	78.8	177.7	113.9	20.5	129.2	116.3	106.3
→3)-α-D-Xyl-(1→	5.38	3.74	3.87	3.69	3.68, 3.95						
b	101.2	73.6	84.4	70.5	63.6						
→3)-β-D-GlcA-(1→	4.72	3.48	3.67	3.75	3.75						
c	105.0	74.4	83.4	74.9	78.2						
→3)-α-D-Xyl-(1→	5.35	3.72	3.86	3.68	3.67, 3.94						
d	101.1	73.6	84.5	70.6	63.6						
β-D-GlcA-(1→	4.69	3.36	3.52	3.49	3.73						
e	104.9	75.8	77.9	74.4	78.2						
dp6 (6 sugar units)											
→3)-β-D-GlcA-MU	5.23	3.75	3.75	3.84	3.94	-	6.28	2.46	7.76	7.13	7.13
a	102.2	73.6	82.9	74.8	78.9	177.7	113.9	20.5	129.2	116.3	106.4
→3)-α-D-Xyl-(1→	5.38	3.73	3.87	3.68	3.67, 3.94						
b	101.2	73.6	84.5	70.5	63.7						
→3)-β-D-GlcA-(1→	4.72	3.47	3.67	3.74	3.75						
c	105.1	74.5	83.5	74.8	78.2						
→3)-α-D-Xyl-(1→	5.34	3.72	3.86	3.67	3.67, 3.94						

d	101.1	73.6	84.5	70.5	63.7
→3)-β-D-GlcA-(1→	4.72	3.47	3.65	3.73	3.73
e	105.1	74.4	83.5	74.8	78.2
α-D-Xyl-(1→	5.31	3.49	3.66	3.57	3.62, 3.89
f	101.3	74.2	75.4	71.8	63.9

[a] Chemical shifts at 15 $^{\circ}$C for all the products except for dp3 which is at 25 $^{\circ}$C.
[b] Assigned based on the overlay of HMQC and HMBC spectra.

References

1. A. Varki *et al*., Eds., *Essentials of Glycobiology* (Cold Spring Harbor Press, Cold Spring Harbor New York, ed. 2, 2009).

2. O. Ibraghimov-Beskrovnaya *et al*., Primary structure of dystrophin-associated glycoproteins linking dystrophin to the extracellular matrix. *Nature* **355**, 696 (1992). doi:10.1038/355696a0 Medline

3. R. Barresi, K. P. Campbell, Dystroglycan: from biosynthesis to pathogenesis of human disease. *J. Cell Sci.* **119**, 199 (2006). doi:10.1242/jcs.02814 Medline

4. T. Yoshida-Moriguchi *et al*., *O*-Mannosyl phosphorylation of alpha-dystroglycan is required for laminin binding. *Science* **327**, 88 (2010). doi:10.1126/science.1180512 Medline

5. C. Longman *et al*., Mutations in the human LARGE gene cause MDC1D, a novel form of congenital muscular dystrophy with severe mental retardation and abnormal glycosylation of alpha-dystroglycan. *Hum. Mol. Genet.* **12**, 2853 (2003). doi:10.1093/hmg/ddg307 Medline

6. C. Godfrey, A. R. Foley, E. Clement, F. Muntoni, Dystroglycanopathies: coming into focus. *Curr. Opin. Genet. Dev.* **21**, 278 (2011). doi:10.1016/j.gde.2011.02.001 Medline

7. M. Kanagawa *et al*., Molecular recognition by LARGE is essential for expression of functional dystroglycan. *Cell* **117**, 953 (2004). doi:10.1016/j.cell.2004.06.003 Medline

8. R. Barresi *et al*., LARGE can functionally bypass alpha-dystroglycan glycosylation defects in distinct congenital muscular dystrophies. *Nat. Med.* **10**, 696 (2004). doi:10.1038/nm1059 Medline

9. J. M. Ervasti, K. P. Campbell, A role for the dystrophin-glycoprotein complex as a transmembrane linker between laminin and actin. *J. Cell Biol.* **122**, 809 (1993). doi:10.1083/jcb.122.4.809 Medline

10. H. Yamada *et al*., Characterization of dp6troglycan-laminin interaction in peripheral nerve. *J. Neurochem.* **66**, 1518 (1996). doi:10.1046/j.1471-4159.1996.66041518.x Medline

11. H. Bakker *et al*., Functional UDP-xylose transport across the endoplasmic reticulum/Golgi membrane in a Chinese hamster ovary cell mutant defective in UDP-xylose Synthase. *J. Biol. Chem.* **284**, 2576 (2009). doi:10.1074/jbc.M804394200 Medline

12. N. B. Schwartz, L. Galligani, P. L. Ho, A. Dorfman, Stimulation of synthesis of free chondroitin sulfate chains by beta-D-xylosides in cultured cells. *Proc. Natl. Acad. Sci. U.S.A.* **71**, 4047 (1974). doi:10.1073/pnas.71.10.4047 Medline

13. P. M. Coutinho, E. Deleury, G. J. Davies, B. Henrissat, An evolving hierarchical family classification for glycosyltransferases. *J. Mol. Biol.* **328**, 307 (2003). doi:10.1016/S0022-2836(03)00307-3 Medline

14. M. Brockington *et al*., Localization and functional analysis of the LARGE family of glycosyltransferases: significance for muscular dystrophy. *Hum. Mol. Genet.* **14**, 657 (2005). doi:10.1093/hmg/ddi062 Medline

15. E. Hohenester, D. Tisi, J. F. Talts, R. Timpl, The crystal structure of a laminin G-like module reveals the molecular basis of alpha-dystroglycan binding to laminins, perlecan, and agrin. *Mol. Cell* **4**, 783 (1999). doi:10.1016/S1097-2765(00)80388-3 Medline

16. A. C. Combs, J. M. Ervasti, Enhanced laminin binding by alpha-dystroglycan after enzymatic deglycosylation. *Biochem. J.* **390**, 303 (2005). doi:10.1042/BJ20050375 Medline

17. P. K. Grewal, P. J. Holzfeind, R. E. Bittner, J. E. Hewitt, Mutant glycosyltransferase and altered glycosylation of alpha-dystroglycan in the myodystrophy mouse. *Nat. Genet.* **28**, 151 (2001). doi:10.1038/88865 Medline

18. D. Harrison *et al*., Crystal structure and cell surface anchorage sites of laminin alpha1LG4-5. *J. Biol. Chem.* **282**, 11573 (2007). doi:10.1074/jbc.M610657200 Medline

19. J. M. Rojek, K. P. Campbell, M. B. Oldstone, S. Kunz, Old World arenavirus infection interferes with the expression of functional alpha-dystroglycan in the host cell. *Mol. Biol. Cell* **18**, 4493 (2007). doi:10.1091/mbc.E07-04-0374 Medline

20. D. E. Michele *et al*., Post-translational disruption of dystroglycan-ligand interactions in congenital muscular dystrophies. *Nature* **418**, 417 (2002). doi:10.1038/nature00837 Medline

21. R. Han *et al*., Basal lamina strengthens cell membrane integrity via the laminin G domain-binding motif of alpha-dystroglycan. *Proc. Natl. Acad. Sci. U.S.A.* **106**, 12573 (2009). doi:10.1073/pnas.0906545106 Medline

22. J. D. Esko, T. E. Stewart, W. H. Taylor, Animal cell mutants defective in glycosaminoglycan biosynthesis. *Proc. Natl. Acad. Sci. U.S.A.* **82**, 3197 (1985). doi:10.1073/pnas.82.10.3197 Medline